nature communications

Article

https://doi.org/10.1038/s41467-024-50926-5

Ocean wave energy harvesting with high energy density and self-powered monitoring system

Received: 7 December 2023

Accepted: 25 July 2024

Published online: 02 August 2024

Check for updates

Ze-Qi Lu[1,2] ✉, Long Zhao[1,2], Hai-Ling Fu[3] ✉, Eric Yeatman[4], Hu Ding[1] & Li-Qun Chen[1]

Constructing a ocean Internet of Things requires an essential ocean environment monitoring system. However, the widely distributed existing ocean monitoring sensors make it impractical to provide power and transmit monitored information through cables. Therefore, ocean environment monitoring systems particularly need a continuous power supply and wireless transmission capability for monitoring information. Consequently, a high-strength, environmentally multi-compatible, floatable metamaterial energy harvesting device has been designed through integrated dynamic matching optimization of materials, structures, and signal transmission. The self-powered monitoring system breaks through the limitations of cables and batteries in the ultra-low-frequency wave environment (1 to 2 Hz), enabling real-time monitoring of various ocean parameters and wirelessly transmitting the data to the cloud for post-processing. Compared with solar and wind energy in the ocean environment, the energy harvesting device based on the defective state characteristics of metamaterials achieves a high-energy density (99 W/m^3). For the first time, a stable power supply for the monitoring system has been realized in various weather conditions (24 h).

Up to 70% of the Earth's surface area is covered by oceans, and the construction of the Ocean Internet of Things (OIoT) by various countries aims to monitor various ocean parameters. However, a key challenge in building OIoT is how to effectively power these widely distributed sensors over the long term[1–3]. These sensors are numerous and widely distributed, with some arranged in extreme environments where battery replacement or power supply via cable is challenging[4–8]. Thus, to ensure a consistent power supply to sensor devices in OIoT, leveraging energy harvesting technology to convert the ocean blue energy offers a self-sustainable solution for long-term and distributed monitoring.

Environmental energy, such as vibration[9–11], friction[12,13], solar[14–16], wind[17,18], and ocean waves[18–22], is harvested and converted into electrical energy by energy harvesting technology. For monitoring devices and sensing networks operating in the ocean, ocean wave energy harvesting offers several advantages, including (1) the highest energy density among all renewable energy sources[23], (2) no chemical pollution to the ocean environment, and (3) a longer average time of availability. Wave energy can be available for up to 90% of the time compared with wind and solar energy, which are typically 20–30%[24]. The development of wave energy harvesting technology has resulted in numerous large harvesting devices, including attenuators[25], oscillating wave surface converters[26], pressure-differential wave energy converters[27], point absorbers[28], operating water columns[29], and bulge head energy converters[30]. Masuda et al.[31] developed a self-powered buoy that utilizes ocean wave energy to navigate ships at sea. While gradually increasing the energy conversion capacity, challenges are

[1]Shanghai Institute of Applied Mathematics and Mechanics, Shanghai Key Laboratory of Mechanics in Energy Engineering, Shanghai Frontier Science Center of Mechanoinformatics, School of Mechanics and Engineering Science, Shanghai University, Shanghai, China. [2]School of Microelectronics, Shanghai University, Shanghai, China. [3]School of Automation, Beijing Institute of Technology, Beijing, China. [4]Department of Electrical and Electronic Engineering, Imperial College London, London, UK. ✉e-mail: luzeqi@shu.edu.cn; hailing.fu@bit.edu.cn

encountered in building and maintaining these large-scale ocean energy harvesting systems due to their bulkiness, complexity, and high costs. Furthermore, limitations were observed in the efficiency of harvesting irregular low-frequency ocean wave energy in these systems. Thus, the development of an innovative and efficient device to overcome the technical limitations of conventional ocean energy harvesting equipment is desirable.

Professor Wang's team proposed an energy harvesting approach in 2012 to address the problems of complex structures and high construction and maintenance costs of large-scale ocean wave energy harvesting equipment. This method is based on the coupling of triboelectrification and electrostatic induction, and it is called triboelectric nano-generator (TENG)[32–34]. The main methods for wave energy harvesting through a triboelectric mechanism include liquid-solid contact TENG[35,36], fully enclosed TENG[37,38], biomimetic structure TENG[39], and ocean energy harvesting TENG network structures[40]. The application of TENG technology has demonstrated highly effective performance for wave and tidal energy, which is prevalent in the ocean[41–43]. However, frictional electro-nano-generators suffer from water ingress and coating damage in special environments, such as typhoons and thunderstorms, resulting in the loss of their ability to convert energy. Thus, an energy harvesting device that is insensitive to the above factors must be designed to ensure a continuous supply of energy to ocean monitoring devices in extreme environments.

Metamaterials exhibit the characteristic of concentrating energy at the defect location[44–47]. Recently, point defect-based metamaterials have gained prominence in the field of vibration energy harvesting[48–54]. Acoustic metamaterials with point defects exhibit an acoustic localization[55] and energy concentration[56] effect at the defect location. The efficiency of vibration energy harvesting is enhanced by the mutual coupling of coupled electrical Helmholtz resonators[57]. External environments, such as temperature[58], affect two-dimensional (2D) infinite metamaterials containing point defects to enhance vibration energy harvesting. Ravanbod et al.[59] designed an efficient piezoelectric harvesting device based on the defect state properties of metamaterials; Akbari-Farahani et al.[60] concentrated the sound energy at the defect locations of metamaterials to enhance the acoustic wave energy harvesting; Krushynska et al.[61] investigated the band gap of metamaterials and designed a single-phase solid metamaterial with a quasi-resonant Bragg band gap that enables the modulation of elastic waves. The studies above share a common feature: the highest vibrational energy is harvested at the defect band frequencies for both elastic and acoustic vibration energy harvesting. Inspired by these primary discoveries, this study proposes an energy harvesting device for point defect metamaterials that can modulate the elastic waves generated during wave fluctuations and concentrate the in-plane fluctuation wave energy at the defect location for efficient energy harvesting.

Conventional TENGs encounter durability challenges, and the organic materials used may decompose because of the effects of salt water and sunlight, resulting in a loss of their ability to generate electricity. Electromagnetic energy harvesters offer the advantages of a simple structure and high shock resistance but suffer from low output voltage. The surface vibration energy is concentrated to form a high-density energy region based on the energy concentration properties of the metamaterial. This improves the output voltage of the energy harvester.The phenomenon of nonuniformity of the output phase may occur when wave energy is harvested using multiple energy harvesting[37,38,62,63] cells in a device, which can significantly reduce the efficiency of wave energy harvesting. Leveraging the defect state properties of metamaterials enables the concentration of wave energy at the defect location when the wave frequency matches the resonance frequency. This mechanism significantly enhances the efficiency of energy harvesting and ensures a sustainable and stable energy supply for the monitoring system.

This study designs a self-powered sensing node for the sensing network in the ocean IoT system, which applies the energy concentration effect of point-deficient metamaterials for efficient wave energy harvesting to supply electrical energy of the sensing nodes for OIoT systems. This device is waterproof, corrosion-resistant, and unaffected by coatings, allowing for more effective harvesting and conversion of wave energy in extreme weather conditions. Compared with traditional ocean wave energy harvesters, the nonlinear electromagnetic energy harvesting device developed in this study offers the benefits of a simple structure, superior shock resistance, and cost-effectiveness. However, electromagnetic energy harvesting devices generate high-induced currents and low voltages, and the magnitude of the electrical output is affected by the rate of change of the magnetic flux. To address this challenge, this study the use of the unique defect state characteristics of metamaterials to harvest the scattered vibration energy within the oceam wave environment at the defect location of the metamaterials. The advantage of this design is that it centralizes energy harvesting at a point on a plane, thereby avoiding the issue of inconsistent AC phase that arises when multiple energy harvesters are placed across the plane. The article first describes the design and operational principle of the self-powered energy ocean environment monitoring system in the ocean IoT. Subsequently, it examines the energy concentration characteristics of the point-defective metamaterials used for the energy harvesting function in this monitoring system. Experiments were conducted in the simulated wave environment and the real ocean environment. Finally, the conclusion is presented in the discussion section.

Results

Self-powered Ocean environmental health monitoring system

The design of a self-powered ocean environmental health monitoring system that converts ocean wave energy into electrical energy is illustrated in Fig. 1. A schematic of the energy-harvesting process of a metamaterial energy-harvesting device in an ocean wave environment is shown in Fig. 1a. The red dashed circle represents the electromagnetic energy harvesting cell (active cell), which mainly consists of the outer shell, the inner shell, the magnetic ball, and the five series-connected induction coils solidly attached to the inner shell, whereas all the other cells on the plane are passive cells (with no energy harvesting capability), which consist of the outer shell and the resonant ball as shown by the blue dashed circle.as shown in Fig. 1a. It is important to note that the outer shell of the energy harvesting cell and the outer shell of the resonant cell have the same dimensions, but the magnetic ball moves in the inner shell with a radius of motion that is smaller than that of the resonance ball, which is a point of defect in the fabrication in metamaterials. Figure 1b(i) illustrates the energy concentration characteristics of defective metamaterials under wave excitation, where the excitation of the metamaterials is concentrated at the defect location to generate a high-energy density zone. The displacement cloud of a metamaterial plate with point defects when subjected to wave excitation is modelled by using finite element method as shown in Fig. 1b(ii). The energy concentrates per unit area at the location of the defects, resulting in an increase in displacement and more energy at the defect location when the metamaterial plate is subjected to out-of-plane excitation. The metamaterial plate consists of 4×4 cells (scalable), including 15 resonant cells without energy harvesting capability and 1 energy harvesting cell, as shown in Fig. 1a. The ball-rolling resonant cells of the periodic array tune the propagation of elastic waves in the metamaterial plate. When the elastic wave propagates in the metamaterial, the resonant cell at the defect is different from that of the entire periodic array, i.e., a local resonance is formed at the defect location, which limits the elastic wave to the defect location and generates a high-energy-density region to realize efficient harvesting of vibration energy. Efficient harvesting

https://doi.org/10.1038/s41467-024-50926-5

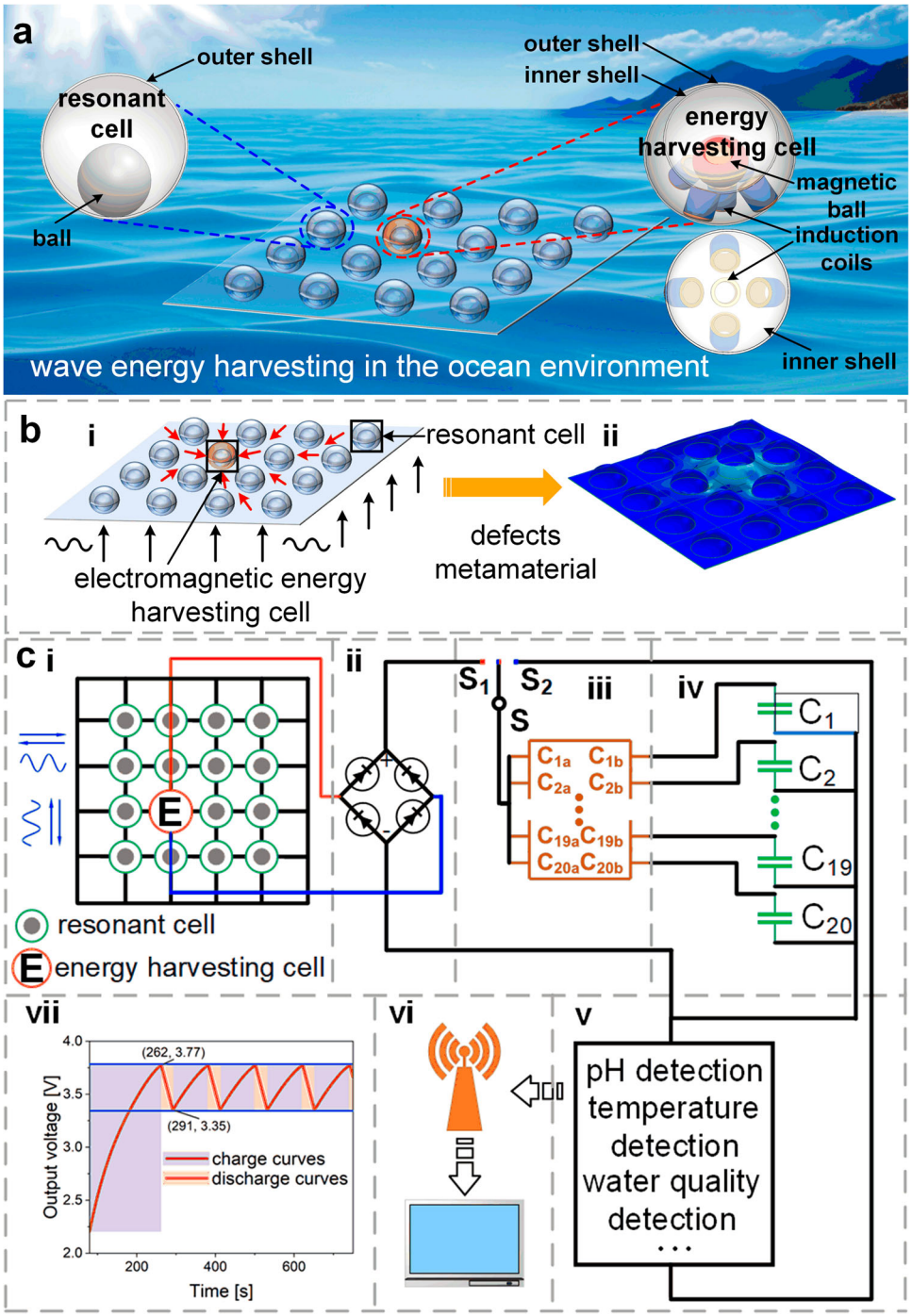

Fig. 1 | Design diagram of wave energy harvesting and self-powered health monitoring system in OIoT. a Schematic of a metamaterial energy harvester harvesting wave energy from the ocean environment.the red dashed circle illustrates the electromagnetic energy harvesting cell and the blue dashed circle illustrates the resonant cell; **b** (i) Schematic of the energy concentration phenomenon of the metamaterial with defects under wave excitation; (ii) Simulated displacement clouds of metamaterial plates with point defects when excited by ocean waves, **c** schematic design of a self-powered ocean environmental health monitoring system: (i) high-density wave energy harvesting metamaterial panels. The green circle illustrates the resonant cell and the red circle illustrates the energy harvesting cell, (ii) rectifier module (AC → DC);(iii) Series/parallel conversion module for energy storage elements. (S is a single-patch double-throw switch (ADG719-EP) integrated into the circuit to achieve series/parallel conversion of the energy storage element. When S_1 is closed, the capacitors are connected in parallel and the energy storage element is charged; when S_2 is closed, the capacitors are connected in series and the energy storage element is discharged); This series/parallel coversion modulue allows the system to be able to charge the storage at low voltages and supply power to sensing subsystems at higher voltages, enhancing the energy harvesting capability; (iv) energy storage module; (v) environmental condition monitoring module (e.g. pH, temperature, and water quality); (vi) monitored information receiving module; and (vii) charge/discharge curves of the energy storage modules.

of wave energy can be realized by placing the harvester in this concentrated zone.

The design of the self-powered ocean environmental health monitoring system is shown in Fig. 1c. Figure 1c (i) and (ii) illustrate the wave kinetic energy harvesting and conversion modules. As illustrated in Fig. 1c(i), an energy-harvesting metamaterial device is placed on the sea surface and driven via the kinetic-potential energy change of wave undulations to convert wave energy into electrical energy.

As illustrated in Fig. 1c(ii), the alternating current (AC) is then converted to direct current (DC) using the rectifier module. As shown in Fig. 1c(iii), the design in this paper adds a new conversion module before the energy storage module, which is used to solve the problem of a single capacitor's low energy storage voltage that cannot drive the monitoring module.The electromagnetic energy harvester can charge multiple storage capacitors at the same time when connected in parallel, and the storage capacitors can output a high voltage when connected in series. Switch S is a single-patch, double-throw (ADG719-EP) switch that is controlled by a chip on the microcontroller. The capacitors (0.1F, 5.5V) are part of a series/parallel conversion module, which comprises multiple double-patch, double-throw (SGM7222YMS10/TR) chips integrated into the microcontroller. When the energy storage module is charging, S_1 is closed, creating a parallel connection between the capacitors. Conversely, when the energy storage module is discharging, S_2 is closed, forming a series connection between the capacitors, providing the monitoring module with a 3.3 V DC voltage. The energy storage module, where several capacitors provide sufficient driving voltage, is illustrated in Fig. 1c(iv). Figure 1c(v) illustrates the ocean environment monitoring module that transmits the monitored data via the wireless module to the receiver module in Fig. 1c(vi). The charging and discharging curves of the energy storage module, which exhibit a cyclic charging and discharging phenomenon after the initial charging is completed, are illustrated in Fig. 1c(vii).

A new conversion module is added in this design before the energy storage module to address the issue of a single capacitor having a low storage voltage and being unable to drive the monitoring module. The capacitors are connected in parallel during charging and in series during discharging, providing sufficient driving voltage for the monitoring module. S_1 is on and S_2 is off during the charging stage. The parallel connection between capacitors and charge C_1, C_2, ...C_{19}, and C_{20}, respectively, is controlled by the serial/parallel conversion modules. S_2 is turned on and S_1 is turned off after charging is complete. The serial/parallel conversion modules regulate the series connection between the capacitors, providing a 3.3 V DC voltage to the monitoring module. The energy storage module, where several capacitors provide sufficient driving voltage, is illustrated in Fig. 1c(v). The charging and discharging curves of the energy storage module, which exhibit a cyclic charging and discharging phenomenon after the initial charging is completed, are illustrated in Fig. 1c(vi). Figure 1c(vii) illustrates the ocean environment monitoring module that transmits the monitored data via the wireless module to the receiver module in Fig. 1c(viii).

Energy concentration characteristics of defective metamaterials

To establish a theoretical foundation for energy-harvesting metamaterial plates with high-density energy regions, the finite element analysis approach was used to examine the response of a periodic array of rolling-ball resonator metamaterial plates at defect locations. This analysis aims to determine the response of the metamaterial plate at the target location when subjected to excitation.

The energy harvesting metamaterial plate, comprising 4 × 4 local resonance cells (0.06 m × 0.06 m each), is shown in Fig. 2a. The structure of the periodic array rolling ball resonance cell and the energy harvesting cell can be seen. Figure 2b illustrates the simple Brillouin region ((Γ-X-M-Γ, Γ-X=X-M)) corresponding to a 2D metamaterial single cell, which is parametrically scanned over the simple Brillouin region for this single cell[44–46]. An electromagnetic energy harvesting cell is placed in a cell, indicated by the red star in Fig. 2c, which serves as an active energy harvesting cell. All other cells were positioned with rolling-ball cells without energy harvesting capability. This configuration creates a defect around the energy harvesting cell, achieving the goal of high-density energy harvesting. Table 1 shows the physical parameters of the metamaterial resonant cell and the energy harvesting cell at the defect location.

A finite element schematic of the 4 × 4 periodic array of the rolling-ball resonator metamaterial plate is illustrated in Fig. 2c. The location of the red pentagram in Fig. 2c signifies the location of the point defect, where the rolling-ball energy harvester from Fig. 1b(i) is positioned to capture the concentrated vibration energy inside the plate. To simulate wave excitation to the plate, a vertical surface excitation (a = 1g) is applied to the lower surface of the metamaterial plate, and the response generated by this excitation is detected at the defect location. This study creates defective bands within the local resonance band gap to achieve metamaterials with energy-concentrating characteristics at ultra-low frequencies. Figure 2d illustrates the theoretical band structures of the point-defect nonlinear local resonance metamaterial. The defect band in the energy band structure can be created by artificially introducing a defect cell (in this study, an energy harvesting cell) into the periodic array cell. The band gap containing the third-order eigenfrequency is the defect band introduced by this defect, as illustrated in Fig. 2d. Within the frequency range of this defect band, the elastic wave propagates through the metamaterial and concentrates at the defect location. The metamaterial exhibits a local resonance band gap at low frequencies (0.9–2 Hz) and a Bragg band gap at higher frequencies (6.7–9.6 Hz). In-plane vibrations of the metamaterial plate are suppressed in the frequency range of the band gap. In particular, the in-plane vibrations of the plate are concentrated at the location of the point defect within the frequency range of the local resonance band gap (0.9–2 Hz), creating a high-energy-density region.

The displacement cloud of the metamaterial plate in the low-frequency range (0.5–3 Hz) is illustrated in Fig. 2e. Figure 2e(i), e(v), and e(vi) are outside the frequency range of the local resonance band gap, whereas Fig. 2e(ii), e(iii), and e(iv) fall within the frequency range of the local resonance band gap. The wave excitation is vertical to the defective metamaterial plate. From the displacement cloud, the resonant balls in each cell roll along the sphere cavities when the metamaterial plate is excited by waves, converting the out-of-plate excitation into in-plate excitation, which is concentrated at the energy harvesting device at the defect location, generating a high-energy-density region at the defect location. A limitation of this design is that the combination of vertical and lateral excitation could result in mistuning of the defect location because of the presence of lateral motion breaking the symmetry. Regarding the metamaterial energy concentration, the best results are achieved when the surface excitation frequency is 1.9 Hz (defective band). This establishes a theoretical basis for subsequently placing a nonlinear electromagnetic energy harvester at the defect location of the metamaterial plate to achieve high-density energy harvesting.

To explore the frequency range of the local resonance defect band, the effect of geometrical parameters on the local resonance band gap of the defective metamaterial plate was examined. Figure 2f illustrates the thickness of the substrate plate, the size of the cell, the size of the outer shell, the size of the resonant ball (essentially the mass),and the plate material. The effect of base-plate thickness on the high-energy density region (local resonant band gap frequency range) of the energy-harvesting metamaterial is illustrated in Fig. 2f(i). Elastic waves propagate through the metamaterial plate when the energy-harvesting metamaterial is excited by ocean waves. For the local resonance band gap, where the high-energy density region is situated, the central frequency of the band gap increases from 1.87 Hz to 1.95 Hz, and the width of the band gap decreases from 0.75 Hz to 0.45 Hz as the thickness of the base plate increases. Consequently, the strength of the energy-harvesting metamaterial plate is increased by increasing the thickness of the base plate. However, the local resonance band gap frequency range decreases, and the high-density energy-harvesting range also decreases, which is not ideal for efficient wave energy harvesting. The effect of the single cell size on the high-energy-density region (local resonance band gap frequency range) of

https://doi.org/10.1038/s41467-024-50926-5

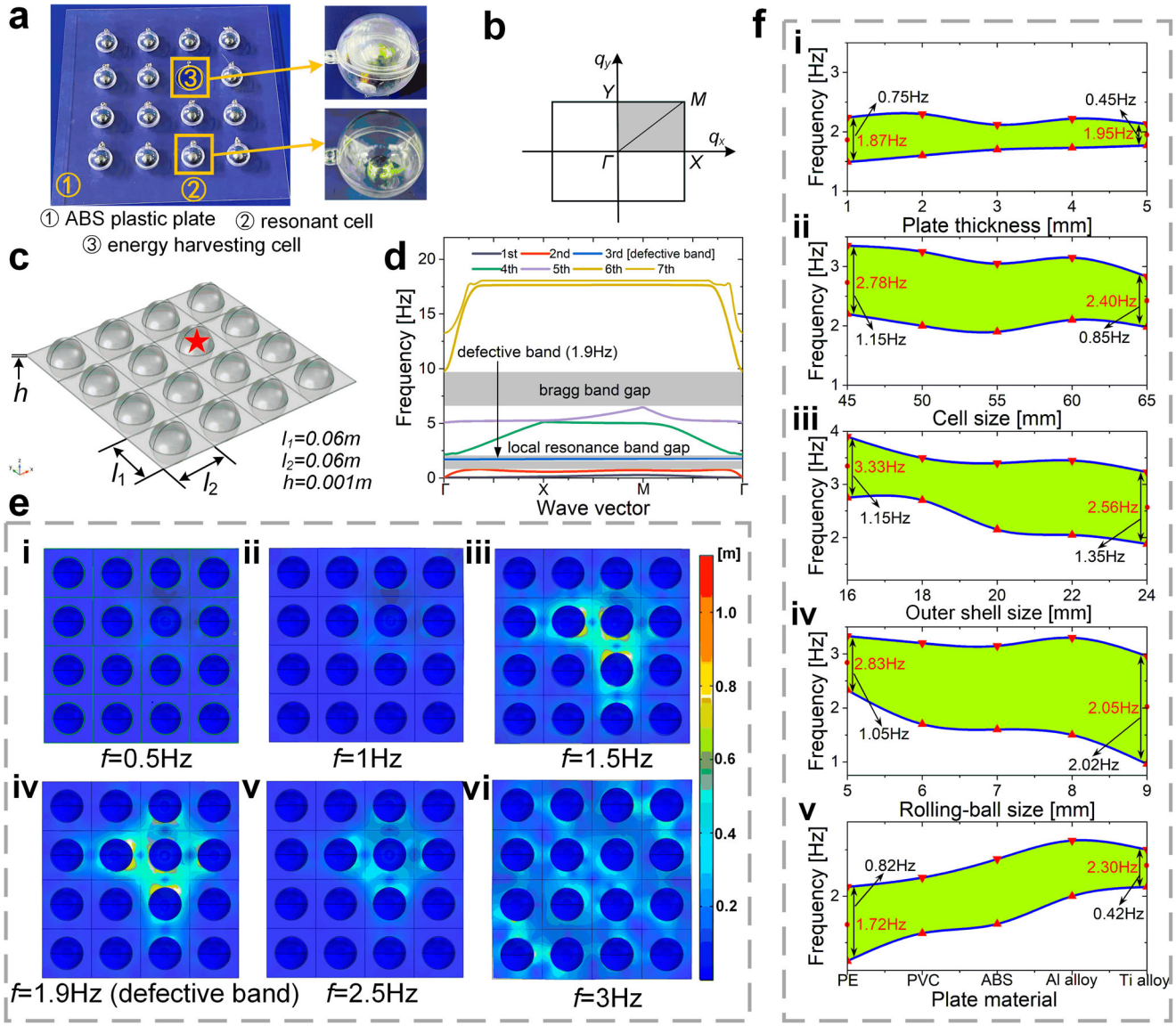

Fig. 2 | Finite element analysis of energy-harvesting metamaterials. a High-density energy-harvesting metamaterial plates (0.3 m × 0.3 m) based on defect characteristics: ① ABS plastic plate; ② resonant cell; ③ energy harvesting cell; **b** simple Brillouin region for two-dimensional metamaterials; **c** finite element model of a defective metamaterial plate; **d** theoretical band structures of defective metamaterial plates; **e** displacement clouds when an acceleration excitation $a = 1g$ is applied to the lower surface of a metamaterial plate containing a point defect: (i) $f = 0.5$ Hz; (ii) $f = 1$ Hz; (iii) $f = 1.5$ Hz; (iv) $f = 1.9$ Hz (Defective band); (v) $f = 2.5$ Hz; (vi) $f = 3$ Hz; **f** effect of geometrical parameters of high-density energy-harvesting metamaterial devices on the frequency range of defect bands: (i) plate thickness; (ii) cell size; (iii) outer shell size; (iv) rolling-ball size; (v) plate material.

the energy-harvesting metamaterial is illustrated in Fig. 2f(ii). As illustrated in Fig. 2f(ii), an increase in the size of the single cell results in a decrease in the band gap width from 1.15 Hz to 0.85 Hz, and the center frequency of the band gap decreases from 2.78 Hz to 2.4 Hz. Although the increase in the size of the single cell has a decreasing effect on the range of the high-energy-density region (local resonance band gap), it reduces the center frequency of the region, aligning most of the frequency range within the band gap with the frequency range of ocean waves. This enables better adaptation to the frequency range of ocean waves and enhances the high-density harvesting of ocean wave energy.

The effect of outer shell size on the high-energy-density region (local resonance band gap frequency range) of the energy-harvesting metamaterial is illustrated in Fig. 2f(iii). As illustrated in Fig. 2f(iii), the width of the local resonant band gap increases from 1.15 Hz to 1.35 Hz and the center frequency of the band gap decreases from 3.33 Hz to 2.56 Hz as the ball outer shell increases. Consequently, increasing the ball outer shell can effectively broaden the high-energy-density region for ocean wave energy harvesting, enabling high-density harvesting of ocean wave energy. The effect of the resonant mass (rolling magnetic ball size) on the high-energy-density region (local resonant band gap frequency range) of the energy-harvesting metamaterial is illustrated in Fig. 2f(iv). The frequency range of the local resonant band gap increases from 1 Hz to 2 Hz, and the center frequency of the band gap decreases from 2.83 Hz to 2.05 Hz as the resonant mass increases. The effect of energy-harvesting metamaterial plate materials on the local resonance band gap is discussed in Fig. 2f(v). The main considerations are Polyethylene (PE, $E = 1$ Gpa, $\rho = 900$ kg/m^3),Polyvinyl Chloride (PVC, $E = 2$ Gpa, $\rho = 1500$ kg/m^3),Acrylonitrile Butadiene Styrene (ABS, $E = 2.5$ Gpa, $\rho = 900$ kg/m^3), Aluminum (Al alloy, $E = 72$ Gpa, $\rho = 2700$ kg/m^3),Titanium (Ti alloy, $E = 116$ Gpa, $\rho = 4500$ kg/m^3).According to the findings presented in Fig. 2f(v), the choice of the metamaterial plate material marginally influences the bandwidth and central frequency of the local resonance band gap. The band gap bandwidth for metamaterials with a non-metallic material substrate is 0.8 Hz, whereas that for those with a

Table 1 | Physical parameters of the metamaterial resonant cell and the energy harvesting cell

Item	Notation [unit]	Value
Metamaterials resonant cell		
Length	l_1(m)	0.06
Width	l_2(m)	0.06
Height	h(m)	0.001
Density of the plate	ρ_p(kg/m^3)	2100
Young's modulus of the plate	E_p(Pa)	7×10^8
Poisson's ratio of the plate	v_p	0.29
Radius of the outer shell	R_b(m)	0.02
Density of the rolling ball	ρ_r(kg/m^3)	7800
Young's modulus of the rolling ball	$m(E_r m^3)$	2.1×10^{11}
Poisson's ratio of the rolling ball	v_r	0.3
Radius of the rolling ball	R_r(m)	0.015
Energy harvesting cell at the defect location		
Induction coil (enameled copper wire)		
Induction coil resistance	R_b(Ω)	0.017
Inductor	R_{ind}(mH)	2
Turns of coil	n	200 × 5
Rolling magnetic balls (NdFeB)		
Radius of the magnetic ball	R_m(m)	0.0075
Radius of the outer shell	R_o(m)	0.02
Radius of the inner shell	R_s(m)	0.015
Magnetic flux density	R(mT)	345

metallic material substrate is 0.5 Hz. However, the center frequency for band gaps using a metallic material substrate reaches 2.3 Hz, which exceeds the frequency range of ocean waves. Considering the buoyancy and strength requirements of wave energy harvesting devices, this study selects ABS as the optimal material for constructing the energy-harvesting device's plate. Therefore, a larger resonant mass results in a wider local resonant band gap and a wider frequency range for high-density energy harvesting of ocean wave energy. In summary, the criteria for the design of the metamaterial plane to achieve high-density energy harvesting include a thin substrate, a large cell, and a heavy resonant mass.

Kinetic behavior and output characteristics of metamaterial energy harvesting device

As illustrated in Fig. 3a, b, the experiments simulated wave excitation in both stable and harsh environments, examining the motion states and energy output voltages of the rolling ball within the energy-harvesting metamaterial device under different wave excitation states. In harsh ocean environments such as typhoons, the acceleration of waves is generally greater than 0.5g[64,65], which is related to many factors such as ocean depth, area, and wave period. The acceleration of waves is used as an index to distinguish stable and harsh ocean wave environments. Table 2 shows the conditions used to simulate different types of ocean wave environments. The experiments revealed that when the water tank's acceleration was less than 0.5g, small stable waves were generated. When the acceleration was 0.5g, large stable waves were generated. When the acceleration was larger than 0.5g, the wave becomes huge. When the acceleration was greater than 2g, the waves in the water tank significantly impacted the metamaterial energy harvesting device, occasionally causing the metamaterial plate to flip over. Thus, in this study, the simulated ocean waves under different excitations are classified as stable waves and harsh waves. When the applied acceleration exceeds 2g, the wave impact on the water tank may cause the metamaterial to break. Consequently, the maximum excitation acceleration is limited to 2g.

The motion state and output voltage of the rolling ball in the metamaterial energy harvester under steady wave environments and harsh wave environments are illustrated in Fig. 3c. The motion analysis of the energy harvester in the point defect metamaterial is mainly discussed around the relative position and velocity of the rolling magnetic ball. The red dotted line in Fig. 3c is the center axis of the rolling magnetic ball energy harvester. This study determines the energy output state of an energy harvester by determining the position and velocity of a rolling magnetic ball relative to the central axis. Figure 3c(i)–c(vi) simulate the motion state and energy output of the rolling ball in the metamaterial energy harvester in a stable wave environment, and Fig. 3c(vii)–c(xii) simulate the motion state and energy output of the rolling ball in the metamaterial energy harvester in a harsh environment. In the output voltage curve, each color block (orange, green, and blue) represents the complete cycle of motion of a rolling magnetic ball in the energy harvesting device. The output response and motion cycle of the green block are used as examples. The motion state and output voltage of the rolling ball in the metamaterial energy harvester under steady wave environments (a<0.5g) and harsh wave environments (a>0.5g) are illustrated in Fig. 3c. The motion analysis of the energy harvester in the point defect metamaterial is mainly discussed around the relative position and velocity of the rolling magnetic ball. The red dotted line in Fig. 3c is the center axis of the rolling magnetic ball energy harvester. This study determines the energy output state of an energy harvester by determining the position and velocity of a rolling magnetic ball relative to the central axis. Figure 3c(i)–c(vi) simulate the motion state and energy output of the rolling ball in the metamaterial energy harvester in a stable wave environment, and Fig. 3c(vii)–c(xii) simulate the motion state and energy output of the rolling ball in the metamaterial energy harvester in a harsh environment. In the output voltage curve, each color block (orange, green, and blue) represents the complete cycle of motion of a rolling magnetic ball in the energy harvesting device. The output response and motion cycle of the green block are used as examples.

As illustrated in Fig. 3c(i), when a wave with $a = 0.1$g and $f = 2$ Hz excites the energy-harvesting metamaterial plate, the plate undergoes slight oscillations against the surface of the wave, inducing the rolling magnetic ball in the electromagnetic energy harvester to roll slightly along the surface of the outer shell and rotate around the center of mass of the magnetic ball. When observing the motion of the metamaterial plate under this excitation, the rolling magnetic ball in the electromagnetic energy harvesting device is divided into two primary states: (1) rolling along the surface of the outer shell, with the sequence B_1-(blue arrow)-A_1-(yellow arrow)-B_1, B_1-(blue arrow)-C_1-(yellow arrow)-B_1, and (2) rotation of the magnetic ball along its center of mass, representing the jittering of the rolling magnetic ball at different positions. Combined with the time domain response signal of the voltage output from the energy harvesting device illustrated in Fig. 3c(ii), in one motion cycle, the kinetic energy of the rolling magnetic ball is converted into potential energy when moving from position B_1 to position C_1, and the output response at position C_1 is 0.Conversely, the potential energy of the rolling magnetic ball is converted into kinetic energy when moving from position C_1 to position B_1, reaching the highest speed at position B_1, and the output response is the largest at 0.07 V. Similarly, when moving from position B_1 to position A_1, the kinetic energy of the rolling ball is converted into potential energy, the speed of the rolling ball gradually decreases to 0, and the induced voltage is 0. The time domain response signal also reveals a "concentrated response" in the output signal range because of the tiny voltages produced by the rolling magnetic ball along its center of mass. In this case, the induced voltage is insufficient to pass through the rectifier, representing the lower limit of the low-power supply. In summary, based on the defective state characteristics of metamaterials, energy-harvesting devices can also generate high densities of induced voltage under the excitation of small waves,

https://doi.org/10.1038/s41467-024-50926-5

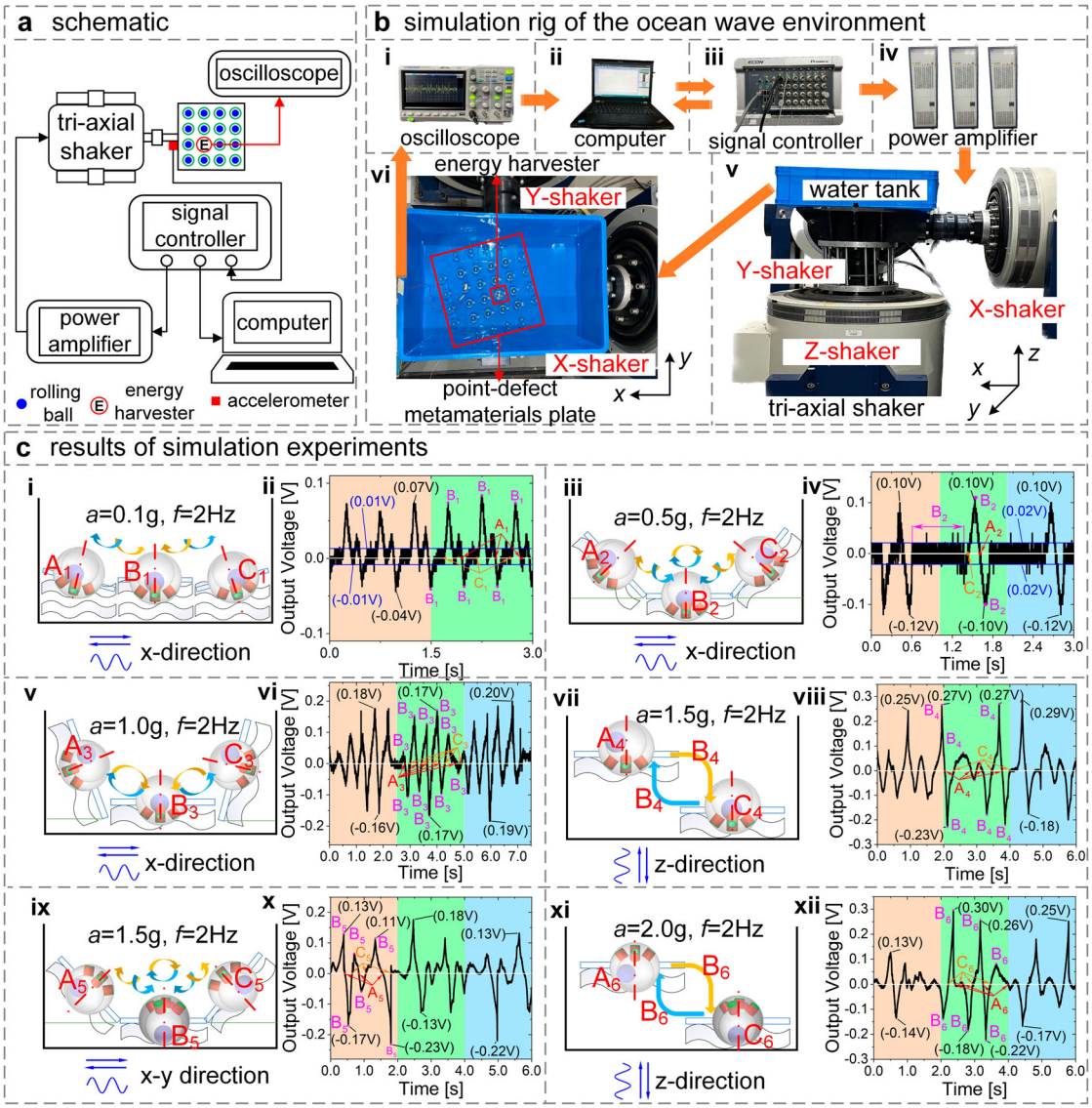

Fig. 3 | Experiments of the response of a high-density energy-harvesting metamaterial device under various wave size conditions. a schematic of the experimental rig; **b** photographs of the experimental rig: (i) oscilloscope, which shows the energy-harvesting metamaterial plate output voltage; (ii) computer; (iii) signal controller, which generates sinusoidal signals; (iv) power amplifier;(v) triaxial shakers that provide excitation in the *x*-, *y*- and *z*-directions;(vi) flume, which simulates the ocean wave environment; **c** motion state analysis and output voltage of a rolling magnetic ball in a metamaterial energy-harvesting device under various wave conditions:(i), (ii): $a = 0.1$ g, $f = 2$ Hz, *x*-direction excitation; (iii), (iv): $a = 0.5$g, $f = 2$ Hz, *x* -direction excitation; (v), (vi): $a = 1.0$ g, $f = 2$ Hz, *x*-direction excitation; (vii), (viii): $a = 1.5$ g, $f = 2$ Hz, *z*-direction excitation; when the energy harvesting metamaterial plate is in the multi-direction excitation state; (ix), (x): $a = 1.5$g, $f = 2$ Hz, *x*-*y*-direction excitation, when the energy harvesting metamaterial plate is in the multi-direction excitation state; (xi), (xii): $a = 2.0$ g, $f = 2$ Hz, *z*-direction excitation, when the energy harvesting metamaterial plate is in the overturning state; where (i)–(vi) simulate the motion state and energy output of the rolling ball in the metamaterial energy harvester in a steady wave environment, (vii)–(xii) simulate the motion state and energy output of the rolling ball in the metamaterial energy harvester in a harsh environment.

efficiently converting small wave energy into electrical energy for low-power devices.

The rolling magnetic ball in the nonlinear electromagnetic energy harvester causes a small rotational jitter around a wave at $a = 0.5$ g and $f = 2$ Hz, as a stable position when the energy-harvesting metamaterial plate is excited, as illustrated in Fig. 3c(iii). The motion of the energy-harvesting metamaterial plate is primarily divided into three states: (1) B_2-(yellow arrow)-A_2-(blue arrow)-B_2; (2) B_2-(yellow arrow)-B_2-(blue arrow)-B_2; (3) B_2-(yellow arrow)-C_2-(blue arrow) -B_2, in a cyclic motion. In the time domain signal illustrated in Fig. 3c(iv), the point marked by C_2 is the output voltage of the energy harvester in the metamaterial plate at state C_2.In this state, the kinetic energy of the rolling magnetic ball is converted into gravitational potential energy, the velocity is 0, the change in magnetic flux in the induction coil is 0, and the induced voltage is 0. Similarly, the point marked by B_2 represents the output voltage of the energy harvester at position B_2.At this time, the gravitational potential energy of the rolling magnetic ball is converted into kinetic energy, the speed is maximum, the rate of change of magnetic flux in the induction coil is maximum, and the induced voltage reaches a peak of 0.1 V. The point marked by A_2 is the output voltage of the electromagnetic energy harvester at position A_2, where the kinetic energy of the rolling magnetic ball is converted into gravitational potential energy. At position A_2, the velocity is 0, the rate of change of the magnetic flux in the induction coil is 0, and the induced voltage is 0. Consequently, under the excitation of small waves, the kinetic energy is converted into electrical energy under the accumulation of

Table 2 | Conditions of the ocean wave environment simulation experiments

Excitation acceleration [g][1]	Excitation direction	Metamaterial plate	Simulation of the ocean wave environment
0.1	*x*-direction	No flip	Stable
0.5	*x*-direction	no flip	Stable
1.0	*x*-direction	no flip	Harsh
1.5	*z*-direction	no flip	Harsh
1.5	*x*-ydirection	flip	Harsh
2.0	*z*-direction	flip	Harsh

[1] In harsh ocean environments such as typhoons, the acceleration of waves is generally greater than 0.5g[64,65], which is related to many factors such as ocean depth, area, and wave period. The acceleration of waves is used as an index to distinguish stable and harsh ocean wave environments.

the kinetic energy of several small waves, resulting in the output voltage varying from -0.1 V to 0.1 V.

As illustrated in Fig. 3c(v), the cyclic motion of the energy-harvesting metamaterial plate occurs in the order B_3-(blue arrow)-A_3-(yellow arrow)-B_3 and B_3-(blue arrow)-C_3-(yellow arrow)-A_3, where the arrow indicates the direction of the rolling magnetic ball movement. Figure 3c(vi) illustrates the time domain signal of the output voltage of the energy-harvesting metamaterial device over 2.5 s. In this time domain, the overall signal can be divided into three large periods, which are then divided into three regions for analysis. The time domain signal of the induced voltage in Fig. 3c(vi) reveals that the maximum value of the induced voltage is 0.17 V throughout the entire stable period.The metamaterial plate demonstrates outstanding energy conversion capabilities when excited by large waves.

To examine the energy output capability of the metamaterial energy harvesting device and the motion of the rolling magnetic ball in the harsh wave environment, Fig. 3c(vii) simulates the state of the metamaterial plate excited by the "surging wave" from the seafloor, when the triaxial shaker applies vertical excitation to the water tank. When the metamaterial plate is excited by the surface of the ocean in the *z*-direction, the motion of the rolling magnetic ball in the energy harvesting device is monitored. Primarily, the rolling magnetic ball performs a jumping motion away from the surface of the inner shell, i.e., A_4-(yellow arrows)-B_4-(yellow arrows)-C_4, and C_4-(blue arrows)-B_4-(blue arrows)-A_4. Compared with the surface of the ocean, the energy harvesting device of the metamaterial plate is at different heights and moments in time. During the jumping process (B_4), the magnetic ball moves at the maximum speed, when the output voltage is maximum, and the output voltage of the energy harvesting device can be up to 0.27 V, as shown in Fig. 3c(viii). When the rolling magnetic ball occupies positions A_4 and C_4, it remains relatively static with respect to the inductive coil, resulting in an instantaneous voltage output of 0 V. Simulating the metamaterial energy harvesting device under vertical excitation of the experiment demonstrates that the device has robust energy harvesting ability even under the harsh ocean environment of "surging wave".

In ocean environments, the energy harvesting device can experience asymmetric excitation from multiple directions, resulting in the flipping of the metamaterial energy harvesting device. Figure 3c(ix) simulates a working condition in which the metamaterial energy harvesting device is subjected to simultaneous $x-y$ multi-directional excitations in a flipped state. Observing the motion of the energy harvesting device reveals that this device undergoes a rotational motion while moving with the wave, and the rolling ball also rotates along the inner wall of the inner shell when the rolling magnetic ball is farther away from the induction coil, i.e., B_5-(yellow arrow)-A_5-(blue arrow)-B_5; B_5-(yellow arrow)-C_5-(blue arrow). In the process of movement, the speed of the rolling magnetic ball relative to the induction coil is maximum in the B_5 state, resulting in the highest instantaneous output voltage of 0.23 V. Conversely, in the A_5 and C_5 states, the speed of the rolling magnetic ball relative to the induction coil is zero, leading to an instantaneous output voltage of 0. In the flip state, as shown in Fig. 3c(x), the output voltage of the metamaterial energy harvesting device decreases. The output voltage of the device in the flip state is 0.23 V. This simulation confirms that the device also exhibits good energy harvesting capability under asymmetric excitation.

Figure 3c(xi) simulates the motion state and energy output capability of the energy harvesting metamaterial plate in the overturning state under ultra-large vertical excitation of a = 2.0 g. This simulated environment is an extremely harsh ocean wave environment when the metamaterial plate is also in the up and down state on the ocean wave surface and the rolling magnetic ball in the energy harvester is in a jumping state. Observing the motion of the energy harvesting device reveals that the rolling magnetic ball and the induction coil are in a relatively stationary state at the A_6 and C_6 moments, resulting in an instantaneous output voltage response of 0, as illustrated in Fig. 3c(xii). At moment B_6, the rolling ball in the energy harvesting device is in a jumping state, and the relative velocity between the rolling magnetic ball and the inductive coil is maximum at this instantand the output voltage reaches 0.3 V. Consequently, given that the excitation of the wave to the energy harvesting device is sufficiently large, the device still maintains a high energy output in the overturning state.

Characterization of a self-powered Ocean environment monitoring system

In this section, previously investigated high-density energy-harvesting metamaterials were used to develop a self-powered ocean environment monitoring system to collect real-time ocean parameters such as temperature, pH, and salinity. An experimental rig of a self-powered ocean health monitoring system that converts wave energy into electrical energy for the normal operation of the monitoring system is illustrated in Fig. 4a. 16 empty balls are placed around the high-density energy-harvesting metamaterial plate to maintain sufficient buoyancy during practical tests. In the test, the wave energy high-density energy harvesting device based on the defective state characteristics of metamaterials was connected to the monitoring device with wires, and the parts were sealed with hot melt adhesive to waterproof the system to ensure the hermeticity of the ocean environmental health detection system. A schematic of the circuit for the self-powered ocean environment monitoring system is illustrated in Fig. 4b. Due to the electromagnetic induction effect, the energy-harvesting device generates an AC voltage when excited by ocean waves. As illustrated in Fig. 4c, the rectifier circuit was used to convert the AC voltage into a DC voltage, which was used to charge the external capacitor C (0.22 F). The flume was excited using a shaker set at a frequency of 2 Hz, and the optimum load resistance R_L in the circuit was set to 6.2 Ω. This section of the experiment aims to measure the time required for the external capacitor C to accumulate the maximum charge and the time it takes for the external capacitor C to release the stored charge under the load resistance R_L after reaching the maximum charge.

As illustrated in Fig. 4c, the entire charging and discharging process takes 794 s. At the initial time, the voltage across both sides of the external capacitor is 0.0165 mV, which is negligible in the analysis. The voltage across the external capacitor increases continuously during the capacitor charging process, reaching a peak voltage of 0.156 V at 282 s. Theoretically, the peak voltage across the external capacitor is determined using the equation $U_{cmax} = 1.2\mathrm{RMS}(U_o) = 0.157\mathrm{V}$, where U_o represents the AC voltage output by the energy-harvesting device when wave excitation is received. After the voltage across the external capacitor reaches its peak, the external capacitor is connected to the load

https://doi.org/10.1038/s41467-024-50926-5

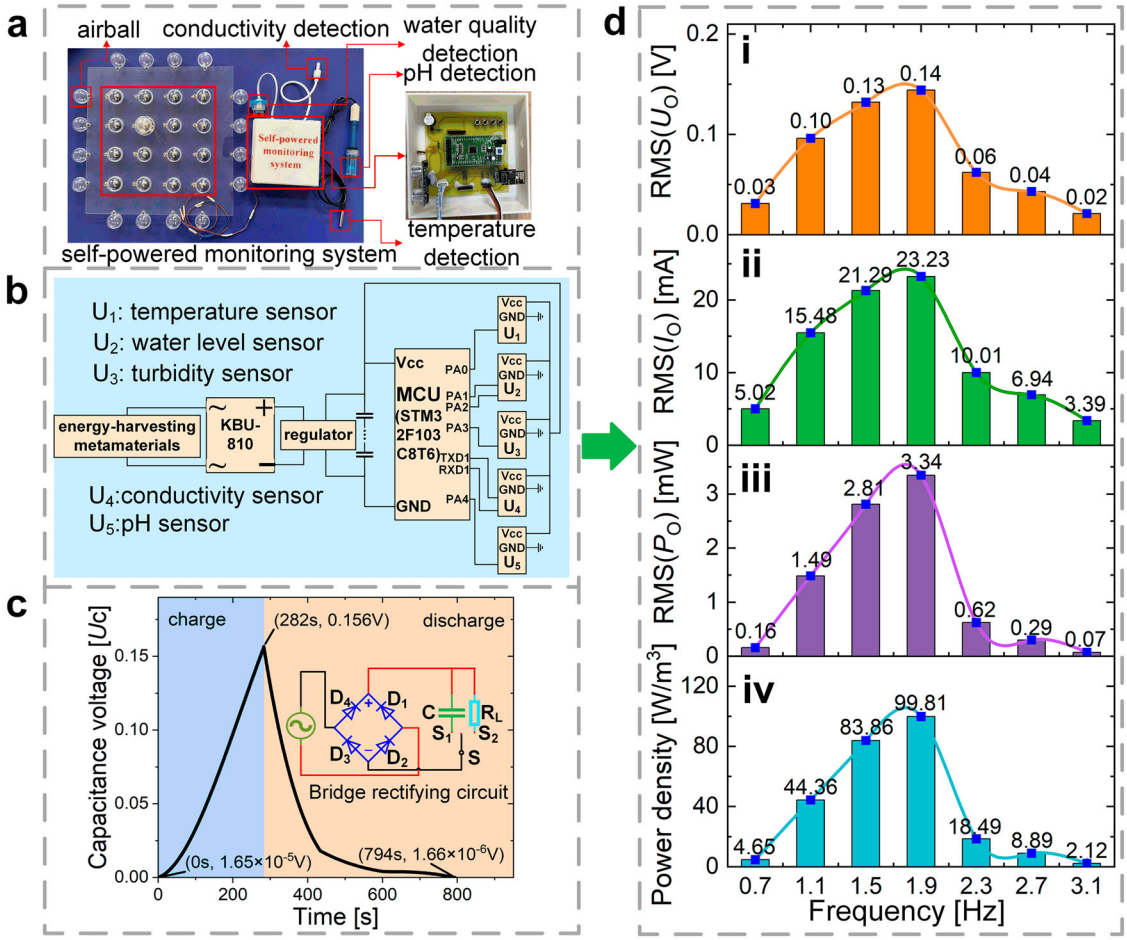

Fig. 4 | Schematic and characterization of a self-powered ocean environment monitoring system. a Schematic of the components of an ocean environment monitoring system for wave energy harvesting by a high-density energy-harvesting metamaterial device (the self-powered energy monitoring system is sealed with hot melt adhesive and the connections between the energy harvesting device and the detection system are waterproofed); **b** Schematic of self-powered ocean environment monitoring system circuits; **c** capacitor charging and discharging experiments and results; **d** Output characterization of energy-harvesting metamaterials at different frequencies: (i) output voltage, (ii) output current, (iii) output power, and (iv) power density.

capacitor R_L for the discharge experiment. As shown in Fig. 4c, the voltage across the external capacitor converges to 0 after 512 s of continuous discharge. The oscilloscope showed a negligible residual voltage of 0.0166 mV across the external capacitor at the end of the discharge experiment. The charge/discharge test demonstrates that the electrical energy generated by the energy-harvesting metamaterial board can be harvested and used when the harvester is excited by waves.

As illustrated in Fig. 4d, the output voltage, current, power, and energy density of the energy-harvesting metamaterial plates were experimentally measured at various wave frequencies. The output power within the band gap frequency significantly exceeds that outside the band gap frequency. Consequently, the output characteristics of the metamaterial energy harvester at 2 and 4 Hz were compared. At a simulated ocean wave frequency of $f = 2$ Hz, which falls within the frequency range of the metamaterial local resonance band gap, the RMS value of the output voltage from the metamaterial energy harvesting device is 0.13 V. At a simulated ocean wave frequency of $f = 4$ Hz, which is outside the frequency range of the metamaterial local resonance band gap, the RMS value of the output voltage is 0.01 V, and the band gap frequency is within the metamaterial energy. The output voltage capability of the harvesting device increased by 1300%. The RMS value of the output power is 2.72 mW at $f = 2$ Hz and 0.01 mW at $f = 4$ Hz. The output power of the energy-harvesting device in the band gap is increased by three orders of magnitude. The unit power density is 81.1 W/m^3 at $f = 2$ Hz and 1.02 W/m^3 at $f = 4$ Hz. The unit power density of the energy-harvesting device in the band gap frequency range was increased by a factor of 80. Therefore, the combination of the high energy density properties of elastic wave localization and the amplification of point-defective metamaterials with an electromagnetic energy harvester can form a new vibration energy harvester, achieving high-performance vibration energy harvesting for powering low-power sensing devices.

Table 3 compares the structural features and energy output capability of the point defect metamaterial energy harvesting device designed in this study with those of existing wave energy harvesting devices in the literature. Table 3 reveals that the point-defect metamaterial energy harvesting device designed in this study exhibits superior harvesting capability for the kinetic energy of low-frequency waves and offers advantages such as very low internal resistance, high output current, simple structure, and absence of chemical coating compared with the existing harvesting device.

Application of a self-powered Ocean environment monitoring system

To validate the monitoring effectiveness of the self-powered ocean environment monitoring system, this section conducts field application tests on the self-powered monitoring system. Figure 5a shows a complete self-powered ocean environment monitoring system, which mainly consists of high-density energy harvesting metamaterials and environment monitoring software. Figure 5b shows the experimental

https://doi.org/10.1038/s41467-024-50926-5

Table 3 | Conditions of the ocean wave environment simulation experiments

Parameters	Mutsuda et al.[10]	Kazemi et al.[11]	Zhang et al.[35]	Rodrigues et al.[36]	This work
Type	piezoelectric	piezoelectric	triboelectric	triboelectric	electromagnetic
Structural feature	painted flexible piezoelectric devices	waterproof piezoelectric wave energy harvester	multi-grating triboelectric nanogenerator	rolling-sphere-based triboelectric nanogenerators	Point-defect metamaterial energy harvester
Load resistance (R_L)	1 MΩ	0.7 MΩ	1 MΩ	30 MΩ	6.2 Ω
Output current (I_o)	0.29 mA	14 μA	27.5 μA	2.8 μA	23.23 mA
Output power (P_o)	87.5 mW	0.15 mW	50 μW	230 μW	3.34 mW
Power density [1]	3.5 W/m^2	158 mW/m^2	4.2 mW/m^2	6.02 mW/m^3	99.81 W/m^3

[1] Comparison of power density: piezoelectric sheet and triboelectric sheet are compared in terms of power density per unit area; triboelectric block and electromagnetic block are compared in terms of power density per unit volume.

photographs of the self-powered ocean environment monitoring system in the day-time and night-time segments of the application. The self-powered ocean environment monitoring system was subjected to real-world environmental experiments in two time periods. The wind speed is 4.5m/s during the daytime from 06:00 to 21:00 and 4.2m/s during the nighttime from 21:00 to 06:00.

To clarify the target frequency of the metamaterial energy harvesting device for realizing the energy concentration phenomenon, the real-time wave height monitoring function of the energy harvesting device was used to derive the wave height monitoring data. The real-time wave height data at 00:00 and 12:00 were Fourier transformed to obtain the ocean wave spectrum, as illustrated Fig. 5c(i and ii) (the red solid line is the instantaneous wave spectrum at 00:00–00:10 and the blue dashed line is the instantaneous wave spectrum at 12:00–12:10). As shown in Fig. 5b, the ocean wave frequencies are distributed within 0.1–2.1 Hz but are primarily concentrated in the frequency ranges of 0.5-1 Hz and 1.5-1.9 Hz. Therefore, the energy concentration frequency of the metamaterial energy harvesting device locates at those frequency ranges, resulting in better energy harvesting efficiency. Figure 5c(iii) shows the spectrum of the output power of the high-density energy harvesting metamaterials. It is found that the output power is maximum near the defect band, with the maximum output power of 21.1 mW and 22.8 mW in the two time periods, respectively. Figure 5d shows the real-time monitoring of ocean information by the ocean environment health monitoring system, which can prove that the self-powered ocean environment monitoring system designed in this work has good practicability.

It is crucial to note that the energy storage device was discharged before the application of the self-powered ocean environment condition monitoring system. As illustrated in Fig. 5a, the energy storage device was used to supply the monitoring system when the energy-harvesting metamaterial plate harvested the wave kinetic energy to charge the energy storage device for 40 min.

Discussion

This study develops a high-density wave energy harvesting device using the defect state properties of metamaterials within the context of ocean wave energy applications. By incorporating energy harvesting defects within the artificial periodic array structure, ocean wave energy in a given area can be harvested more effectively. This involves channeling the wave energy into the energy harvesting device located at the metamaterial defects.

The findings demonstrate that for waves in the local resonance frequency range, an energy-harvesting device based on the defective state properties of metamaterials can efficiently harvest wave energy in the plane. Under different wave excitations, the electromagnetic energy-harvesting device in the metamaterial plate exhibits various states of motion: (a) Under very small wave excitation, the rolling magnetic ball within the electromagnetic energy-harvesting device undergoes a low-amplitude rolling motion along the cavity and rotates around its center of mass. This indicates that the energy-harvesting device based on the defective state properties of the metamaterial produces induced voltages even with very small wave excitation; (b) under stable wave environment excitation, a “complex” nonlinear periodic phenomenon is generated, resulting in the rolling ball generating a peak induced voltage because of the accumulation of wave kinetic energy; (c) under harsh wave environment excitation, the rolling magnetic ball exhibits vigorous movement, while the metamaterial energy harvester demonstrates exceptional energy conversion capabilities.The output power and charge/discharge tests indicate that the energy-harvesting metamaterial device can convert wave energy into electrical energy for harvesting and use. To provide technical support for establishing an ocean environment monitoring network, an OIoT self-powered environment monitoring system cell is designed.

https://doi.org/10.1038/s41467-024-50926-5

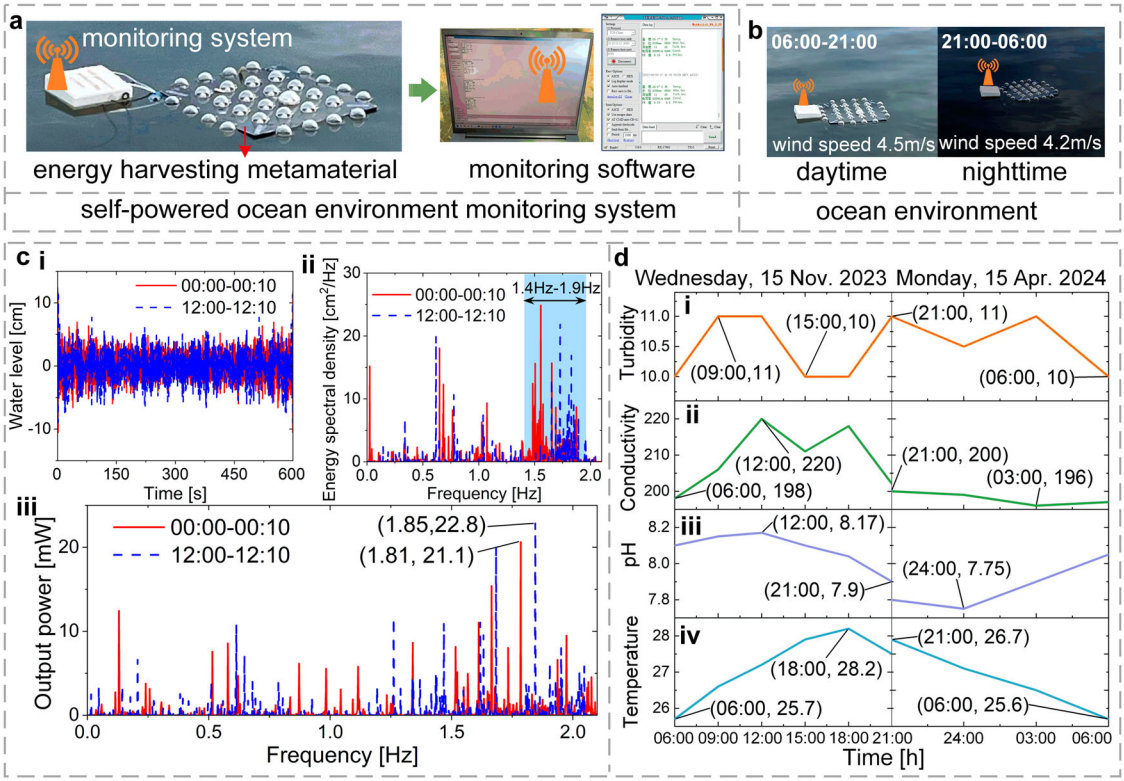

Fig. 5 | Self-powered ocean environment monitoring system. a Self-powered ocean environment monitoring system (High-density energy harvesting metamaterials and environmental monitoring software); **b** the real ocean environment: daytime test environment (wind speed of 4.5 m/s) and nighttime test environment (wind speed of 4.2 m/s); **c** testing results (red solid line: 00:00–00:10; blue dotted line: 12:00–12:10): (i) spectrum of the wave level; (ii) energy spectral density of the wave; (iii) Output power spectrum of the high-density energy harvesting metamaterial; **d** Real-time health monitoring results of the ocean environment in one day: (i) turbidity, (ii) conductivity, (iii) pH, and (iv) temperature.

Methods

Theoretical methods

As illustrated in Fig. 6, the nonlinear energy-harvesting cell is modeled and analyzed to study its energy-harvesting performance. By analyzing the motion state of the rolling magnetic ball, the following equations of motion can be obtained

$$T = T_{\text{tans}} + T_{\text{rot}} = \frac{7}{10} m_1 R_{\text{m}}^2 \left(\left(\frac{d\theta}{dt} \right)^2 + \sin^2(\theta) \left(\frac{d\phi}{dt} \right)^2 \right) \tag{1}$$

where R_θ represents the trajectory of the rolling magnetic ball in the XOZ plane when the rotation angle of the magnetic ball from the center of the ball is θ, R_{b} represents the radius of the inner shell, and R_{m} represents the radius of the magnetic ball, T_{trans} is the translational kinetic energy and T_{rot} is the rotational kinetic energy, and the mass of the rolling magnetic ball is represented by m_1.

In the trajectory of the magnetic ball in the energy harvesting cell, as illustrated in Fig. 1b(i), the potential energy U can be expressed as follows

$$U = m_1 g R_{\text{b}} (1 - \cos(\theta)) \tag{2}$$

According to Lagrange's equation and Kirchhoff's law, the Lagrangian function is expressed as follows

$$\begin{cases} \frac{d}{dt}\left(\frac{\partial(T-U)}{\partial\dot{\theta}}\right) - \frac{\partial(T-U)}{\partial\theta} = -\beta_\theta i - \mu_\theta \frac{d\theta}{dt} \\ \frac{d}{dt}\left(\frac{\partial(T-U)}{\partial\dot{\phi}}\right) - \frac{\partial(T-U)}{\partial\phi} = -\beta_\phi i - \mu_\phi \frac{d\phi}{dt} \\ \frac{di}{dt} + \frac{R_{\text{L}}}{L_{\text{ind}}} i + \frac{BL_{\text{coil}}R_{\text{b}}}{L_{\text{ind}}} \left(\sqrt{\left(\frac{d\theta}{dt}\right)^2 + \left(\frac{d\phi}{dt}\right)^2} \right) = 0 \end{cases} \tag{3}$$

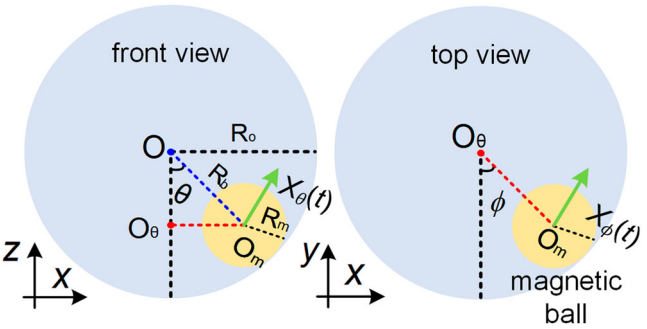

Fig. 6 | Theoretical modeling of nonlinear ball-pendulum energy harvesters.

where β_θ and β_ϕ are the electromagnetic coefficients in the θ and ϕ directions, respectively; μ_θ and μ_ϕ are the damping coefficients in the θ and ϕ directions, respectively; and i is the induced current generated in the coil.

Substituting the above equation into the Lagrange equation, the dynamical equations of the nonlinear energy harvesting cell is

$$\begin{cases} \frac{7}{5} m_1 R_{\text{m}} \frac{d^2\theta}{dt^2} - m_1 g \sin(\theta) + m_1 R_{\text{m}} \sin(\theta)\cos(\theta) \left(\frac{d\phi}{dt}\right)^2 = -\beta_\theta i - \mu_\theta \frac{d\theta}{dt} \\ \frac{7}{5} m_1 R_{\text{m}} \sin^2(\theta) \frac{d^2\phi}{dt^2} = -\beta_\phi i - \mu_\phi \frac{d\phi}{dt} \\ \frac{di}{dt} + \frac{R}{L_{\text{ind}}} i + \frac{BL_{\text{coil}}R_{\text{b}}}{L_{\text{ind}}} \left(\sqrt{\left(\frac{d\theta}{dt}\right)^2 + \left(\frac{d\phi}{dt}\right)^2} \right) = 0 \end{cases} \tag{4}$$

Experimental methods

As illustrated in Fig. 3, a dynamic experiment was conducted to predict the dynamic response of the system under steady-state excitation in a simulated ocean wave environment. The device ECON PREMAX generates the harmonic excitation signal, which is then amplified by the power amplifier MPA407 and fed to the exciter ETS SOLUTIONS M437A, ultimately driving the vibration of the substrate plate carrying the water flume. PCB PIEZOTRAONICS sensors collect the vibration response. To control the constant amplitude vibration output, the vibration signals collected on the base plate are fed back to the signal generator. The collected signals are filtered to reduce interference from spurious waves[50,51]. The output signal of this experiment is closed-loop controlled to ensure that the excitation is constant with the water flume.

Calculation method of power density

In this manuscript, after obtaining the output voltage of the energy harvesting metamaterial plate at different frequencies, the current in the line can be obtained according to Ohm's law. The output power of the energy harvesting metamaterial plate can be obtained according to the electric power equation. Finally, the power density of the energy harvester is obtained by dividing the output power with the volume of the energy harvesting metamaterial plate.

Manufacture of the metamaterial with defect

To fabricate point-defect metamaterials with energy-concentrating effects, the manufacturing processing of 3D-printing metamertial was employed. Firstly, the resonant cell was fabricated by combining one shell and one free-rolling ball. Then the produced resonant cells were periodically arrayed on a substrate to constitute a metamaterial with a low-frequency local resonant band gap. Then, one of the resonant cells was selected as the energy harvesting cell, which was modified by adding an inner shell, placing a free-rolling magnetic ball inside the inner shell and fixing five series-connected induction coils outside the inner shell. The energy harvesting cell had the same shell diameter compared with other resonant cells. The produced point-defect metamaterial exhibited the energy concentration effect.

Data availability

The source data associated with each of the figures generated in this paper are provided in the source data files. The source data generated in this study have been deposited in the Zenodo database under accession code https://doi.org/10.5281/zenodo.12747434. Source data are provided with this paper.

Code availability

Codes for generating all the results are available from the corresponding authors on request.

References

1. Zhu, H. W. et al. A miniaturized bionic ocean-battery mimicking the structure of marine microbial ecosystems. *Nat. Commun.* **13**, 5608 (2022).
2. Jin, L., Deng, W. L., Su, Y. C. & Zhong, X. Self-powered wireless smart sensor based on maglev porous nanogenerator for train monitoring system. *Nano Energy* **38**, 185–192 (2017).
3. Ellabban, O., Abu-Rub, H. & Blaabjerg, F. Renewable energy resources: current status, future prospects and their enabling technology. *Renew. Sustain. Energy Rev.* **39**, 748–764 (2014).
4. Russell, J. Ocean sensors can track progress on climate goals. *Nature* **15**, 555 (2018).
5. Salter, S. H. Wave power. *Nature* **249**, 720 (1974).
6. Tollefson, J. Power from the oceans: blue energy. *Nature* **508**, 302–304 (2014).
7. Xia, Y. F. et al. Wireless-controlled, self-powered, and patterned information encryption display system based on flexible electroluminescence devices. *Nano Energy* **102**, 10765 (2022).
8. Tuoi, T. T. K., Toan, N. V. & Ono, T. Self-powered wireless sensing system driven by daily ambient temperature energy harvesting. *Appl. Energy* **311**, 118679 (2022).
9. Eghbali, P., Younesian, D., Moayedizadeh, A. & Ranjbar, M. Study in circular auxetic structures for efficiency enhancement in piezoelectric vibration energy harvesting. *Sci. Rep.* **10**, 16338 (2020).
10. Mutsuda, H. et al. A painting type of flexible piezoelectric device for ocean energy harvesting. *Appl. Ocean Res.* **68**, 182–193 (2017).
11. Kazemi, S., Nili-Ahmadabadi, M., Tavakoli, M. R. & Tikani, R. Energy harvesting from longitudinal and transverse motions of sea waves particles using a new waterproof piezoelectric waves energy harvester. *Renew. Energy* **179**, 528–536 (2021).
12. Li, X. M. et al. Kinetic drop friction. *Nat. Commun.* **14**, 4571 (2023).
13. Feng, L. et al. Hybridized nanogenerator based on honeycomb-like three electrodes for efficient ocean wave energy harvesting. *Nano Energy* **47**, 217–23 (2018).
14. Lewis, N. S. Research opportunities to advance solar energy utilization. *Science* **351**, (2016).
15. Chen, J. et al. Micro-cable structured textile for simultaneously harvesting solar and mechanical energy. *Nat. Energy* **1**, 16138 (2016).
16. Zhang, Q. et al. Shadow enhanced self-charging power system for wave and solar energy harvesting from the ocean. *Nat. Commun.* **12**, 616 (2021).
17. Kan, J. W. et al. Energy harvesting from wind by an axially retractable bracket-shaped piezoelectric vibrator excited by magnetic force. *Energy* **240**, 122495 (2021).
18. Lu, Z., Wen, Q., He, X. & Wen, Z. Y. A flutter-based electromagnetic wind energy harvester: theory and experiments. *Appl. Sci.* **9**, 4823 (2019).
19. Ahmed, A. et al. Self-powered wireless sensor node enabled by a duck-shaped triboelectric nanogenerator for harvesting water wave energy. *Adv. Energy Mater.* 1601705 (2016).
20. Khan, U. & Kim, S.-W. Triboelectric nanogenerators for blue energy harvesting. *ACS Nano* **10**, 6429–6432 (2016).
21. Sun, P. D., Xu, B. & Wang, J. C. Long-term trend analysis and wave energy assessment based on ERA5 wave reanalysis along the Chinese coastline. *Appl. Energy* **324**, 119709 (2022).
22. Arguil'e-P'erez, B., Ribeiro, A. S., Costoya, X., deCastro, M. & Gomez-Gesteira, M. Suitability of wave energy converters in northwestern Spain under the near future winter wave climate. *Energy* **278**, 127957 (2023).
23. Alain, C. et al. Wave energy in Europe: current status and perspectives. *Renew. Sustain. Energy Rev.* **6**, 405–431 (2002).
24. Xiao, H. et al. Study of a novel rotational speed amplified dual turbine wheel wave energy converter. *Appl. Energy* **301**, 117423 (2021).
25. Yin, K. et al. Numerical investigation of submerged flexible vegetation dynamics and wave attenuation under combined waves and following currents. *Ocean Eng.* **278**, 114437 (2023).
26. Cheng, Y. et al. Feasibility of integrating a very large floating structure with multiple wave energy converters combining oscillating water columns and oscillating flaps. *Energy* **274**, 127301 (2023).
27. Algie, C., Ryan, S. & Fleming, A. Predicted power performance of a submerged membrane pressure-differential wave energy converter. *Int. J. Mar. Energy* **20**, 125–134 (2017).

28. Budar, K. & Falnes, J. A resonant point absorber of ocean-wave power. *Nature* **256**, 478–479 (1975).
29. Ciappi, L. et al. Wave-to-wire models of wells and impulse turbines for oscillating water column wave energy converters operating in the Mediterranean Sea. *Energy* **238**, 121585 (2022).
30. Zhang, H. & Aggidis, G. A. Nature rules hidden in the biomimetic wave energy converters. *Renew. Sustain. Energy Rev.* **97**, 28–37 (2018).
31. Masuda, Y. et al. Regarding BBDB wave power generation plant. In *Proc. of 2nd European Wave Power Conference*, 69–76 (1995).
32. Wang, Z. L. Catch wave power in floating nets. *Nature* **542**, 159–60 (2017).
33. Cheng, T. H., Shao, J. J. & Wang, Z. L. Triboelectric nanogenerators. *Nat. Rev. Methods Prim.* **3**, 39 (2023).
34. Wang, H. M., Xu, L., Bai, Y. & Wang, Z. L. Pumping up the charge density of a triboelectric nanogenerator by charge-shuttling. *Nat. Commun.* **11**, 4203 (2020).
35. Zhang, D., Shi, J., Si, Y. & Li, T. Multi-grating triboelectric nanogenerator for harvesting low-frequency ocean wave energy. *Nano Energy* **61**, 132–140 (2019).
36. Rodrigues, C. et al. Integrated study of triboelectric nanogenerator for ocean wave energy harvesting: performance assessment in realistic sea conditions. *Nano Energy* **84**, 105190 (2021).
37. Li, X. et al. Networks of high performance triboelectric nanogenerators based on liquid-solid interface contact electrification for harvesting low-frequency blue energy. *Adv. Energy Mater.* **8**, 1800705 (2018).
38. Wang, X. et al. Triboelectric nanogenerator based on fully enclosed rolling spherical structure for harvesting low-frequency water wave energy. *Adv. Energy Mater.* **5**, 1501467 (2015).
39. Zhang, Y. R., Cao, X. & Wang, Z. L. The sealed bionic fishtail-structured TENG based on anticorrosive paint for ocean sensor systems. *Nano Energy* **108**, 108210 (2023).
40. Song, C. H. et al. Recent advances in ocean energy harvesting based on triboelectric nanogenerators. *Sustain. Energy Technol. Assess.* **53**, 102767 (2022).
41. Zi, Y. L. et al. Standards and figure-of-merits for quantifying the performance of triboelectric nanogenerators. *Nat. Commun.* **6**, 8376 (2015).
42. Xia, K., Fu, J. & Xu, Z. Multiple-frequency high-output triboelectric nanogenerator based on a water balloon for all-weather water wave energy harvesting. *Adv. Energy Mater.* **10**, 2000426 (2020).
43. Luo, J. J. et al. Flexible and durable wood-based triboelectric nanogenerators for self-powered sensing in athletic big data analytics. *Nat. Commun.* **10**, 5147 (2019).
44. Liu, Z. Y. et al. Locally resonant sonic materials. *Science* **289**, 1734 (2000).
45. Molero'n, M. & Daraio, C. Acoustic metamaterial for subwavelength edge detection. *Nat. Commun.* **6**, 8037 (2015).
46. Park, C. M. & Lee, S. H. Zero-reflection acoustic metamaterial with a negative refractive index. *Sci. Rep.* **9**, 3372 (2019).
47. Pelat, A., Gallot, T. & Gautier, F. On the control of the first Bragg band gap in periodic continuously corrugated beam for flexural vibration. *J. Sound Vib.* **446**, 249–262 (2019).
48. El-Borgi, S. et al. Multiple bandgap formation in a locally resonant linear metamaterial beam: theory and experiments. *J. Sound Vib.* **488**, 115647 (2020).
49. Xu, J. H. et al. Acoustic metamaterials-driven transdermal drug delivery for rapid and on-demand management of acute disease. *Nat. Commun.* **14**, 869 (2023).
50. Lu, Z. Q., Zhao, L., Ding, H. & Chen, L. Q. A dual-functional metamaterial for integrated vibration isolation and energy harvesting. *J. Sound Vib.* **509**, 116251 (2021).
51. Zhang, J. et al. Remote whispering metamaterial for non-radiative transceiving of ultra-weak sound. *Nat. Commun.* **12**, 3670 (2021).
52. Park, C. S., Shin, Y. C. & Jo, S. H. Two-dimensional octagonal phononic crystals for highly dense piezoelectric energy harvesting. *Nano Energy* **57**, 327–337 (2019).
53. Jiao, P. C., Mueller, J., Raney, J. R., Zheng, X. Y. & Alavi, A. H. Mechanical metamaterials and beyond. *Nat. Commun.* **14**, 6004 (2023).
54. Lezhennikova, K. et al. Experimental evidence of Förster energy transfer enhancement in the near field through engineered metamaterial surface waves. *Commun. Phys.* **6**, 229 (2023).
55. Qi, S. B., Oudich, M., Li, Y. & Assouar, B. Acoustic energy harvesting based on a planar acoustic metamaterial. *Appl. Phys. Lett.* **108**, 263501 (2016).
56. Lv, H., Tian, X. Y., Wang, M. Y. & Li, D. C. Vibration energy harvesting using a phononic crystal with point defect states. *Appl. Phys. Lett.* **102**, 034103 (2013).
57. Yang, A. C. et al. Enhanced acoustic energy harvesting using coupled resonance structure of sonic crystal and Helmholtz resonator. *Appl. Phys. Express* **6**, 127101 (2013).
58. Aly, A. H., Nagaty, A., Khalifa, Z. & Mehaney, A. The significance of temperature dependence on the piezoelectric energy harvesting by using a phononic crystal. *J. Appl. Phys.* **123**, 185102 (2018).
59. Ravanbod, M., Ebrahimi-Nejad, S. Perforated auxetic honeycomb booster with reentrant chirality: a new design for high-efficiency piezoelectric energy harvesting. *Mech. Adv. Mater. Struct.* 1–16 (2023).
60. Akbari-Farahani, F. & Ebrahimi-Nejad, S. From defect mode to topological metamaterials: a state-of-the-art review of phononic crystals & acoustic metamaterials for energy harvesting. *Sens. Actuators A: Phys.* **114871**, 365 (2024).
61. Krushynska, A.O., Miniaci, M., Bosia, F. & Pugno, N.M. Coupling local resonance with Bragg band gaps in single-phase mechanical metamaterials. *Extreme Mech. Lett.* 30–36 (2017).
62. Wang, D. Y., Wang, X. X., Jin, M. L., He, P. & Zhang, S. Y. Molecular level manipulation of charge density for solid-liquid TENG system by proton irradiation. *Nano Energy* **103**, 107819 (2022).
63. Lv, S. S., Zhang, X., Huang, T., Yu, H. & Zhu, M. F. Interconnected array design for enhancing the performance of an enclosed flexible triboelectric nanogenerator. *Nano Energy* **89**, 106476 (2021).
64. Liu, C., Dong, Z., Zhou, Y. & Pan, Y. A computation method for the typhoon waves using the field wave spectrum. *Sustainability* **14**, 7347 (2022).
65. Holthuijsen, L.H. *Waves in Oceanic and Coastal Waters* (Cambridge: Cambridge University Press, 2007).

Acknowledgements

This study was funded by the National Natural Science Foundation of China (Grant Nos. 12272210 and 11872037 to Z.-Q.L.; Grant No. 11572182 to L.-Q.C.) and the Innovation Program of Shanghai Municipal Education Commission (Grant No. 2017-01-07-00-09- E00019 to L.-Q.C.).

Author contributions

Z.-Q.L.: Research concept, Data analysis and interpretation; L.Z.: Design, Writing the article; H.-L.F.: Improving the article; E.Y.: Improving the article; H.D.: Collection; L.-Q.C.: Critical revision of the article, Final approval of article. All authors contributed to discussions.

Competing interests

The authors declare no competing interests.

Additional information

Supplementary information The online version contains supplementary material available at https://doi.org/10.1038/s41467-024-50926-5.

Correspondence and requests for materials should be addressed to Ze-Qi Lu or Hai-Ling Fu.

Peer review information *Nature Communications* thanks Salman Ebrahimi-Nejad, Reza Rashidi and the other, anonymous, reviewer(s) for their contribution to the peer review of this work. A peer review file is available.